Proc. Natl. Acad. Sci. USA
Vol. 88, pp. 3569–3573, May 1991
Biochemistry

The contribution of DNA single-stranded order to the thermodynamics of duplex formation

GORAZD VESNAVER AND KENNETH J. BRESLAUER*

Department of Chemistry, Rutgers, The State University of New Jersey, New Brunswick, NJ 08903

Communicated by Julian M. Sturtevant, January 24, 1991 (received for review November 27, 1990)

ABSTRACT **We report a direct determination of the thermodynamic contribution that DNA single-stranded order makes to DNA duplex formation. By using differential scanning calorimetry (DSC) and temperature-dependent UV absorbance spectroscopy, we have characterized thermodynamically the thermally induced disruption of the 13-mer duplex [d(CGCATGAGTACGC)]·[d(GCGTACTCATGCG)] (henceforth called $S_1 \cdot S_2$) and its component single strands, [d(CGCATGAGTACGC)] (henceforth called S_1) and [d(GCGTACTCATGCG)] (henceforth called S_2). These spectroscopic and calorimetric measurements yield the following thermodynamic profiles at 25°C: $\Delta G° = 20.0$ kcal/mol, $\Delta H° = 117.0$ kcal/mol, and $\Delta S° = 325.4$ cal·degree^{-1}·mol^{-1} for duplex melting of $S_1 \cdot S_2$; $\Delta G° = 0.45$ kcal/mol, $\Delta H° = 29.1$ kcal/mol, and $\Delta S° = 96.1$ cal·degree^{-1}·mol^{-1} for single-strand melting of S_1; $\Delta G° = 1.44$ kcal/mol, $\Delta H° = 27.2$ kcal/mol, and $\Delta S° = 86.4$ cal·degree^{-1}·mol^{-1} for single-strand melting of S_2 (1 cal = 4.184 J). These data reveal that the two single-stranded structures S_1 and S_2 are only marginally stable at 25°C, despite exhibiting rather substantial transition enthalpies. This behavior results from enthalpy and entropy contributions of similar magnitudes that compensate each other, thereby giving rise to relatively small free energies of stabilization for the single strands at 25°C. By contrast, the $S_1 \cdot S_2$ duplex state is very stable at 25°C since the favorable transition entropy associated with duplex disruption (325.4 cal·degree^{-1}·mol^{-1}) is more than compensated for by the extremely large duplex transition enthalpy (117.0 kcal/mol). We also measured directly an enthalpy change ($\Delta H°$) of −56.4 kcal/mol for duplex formation at 25°C using isothermal batch-mixing calorimetry. This duplex formation enthalpy of −56.4 kcal/mol at 25°C is very different in magnitude from the duplex disruption enthalpy of 117.0 kcal/mol measured at 74°C by DSC. Since the DSC measurement reveals the net transition heat capacity change to be close to zero, we interpret this large disparity between the enthalpies of duplex disruption and duplex formation as reflecting differences in the single-stranded structures at 25°C (the initial states in the isothermal mixing experiment) and the single-stranded structures at ≈80°C (the final states in the DSC experiment). In fact, the enthalpy for duplex formation at 25°C (−56.4 kcal/mol) can be combined with the sum of the integral enthalpies required to melt each single strand from 25 to 80°C (23.6 kcal/mol for S_1 and 27.2 kcal/mol for S_2) to calculate a $\Delta H°$ of −107.2 kcal/mol for the hypothetical process of duplex formation from "random-coil" "unstacked" single strands at 25°C. The magnitude of this predicted $\Delta H°$ value for duplex formation is in good agreement with the corresponding parameter we measure directly by DSC for duplex disruption (117.0 kcal/mol), thereby lending credence to our interpretation and analysis of the data. Thus, our results demonstrate that despite being only marginally stable at 25°C, single strands can exhibit intramolecular interactions that enthalpically poise them for duplex formation. For the duplex studied herein, prior to association at 25°C, the two complementary single strands already possess >40% of the total enthalpy (50.8/117) that ultimately stabilizes the final duplex state. This feature of single-stranded structure near room temperature can reduce significantly the enthalpic driving force one might predict for duplex formation from nearest-neighbor data, since such data generally are derived from measurements in which the single strands are in their random-coil states. Consequently, potential contributions from single-stranded structure must be recognized and accounted for when designing hybridization experiments and when using isothermal titration and/or batch mixing techniques to study the formation of duplexes and higher-order DNA structures (e.g., triplexes, tetraplexes, etc.) from their component single strands.**

The existence of ordered structure in oligo- and polynucleotide single strands has been known for some time and has stimulated considerable research designed to elucidate the detailed nature of the forces that give rise to such single-stranded order, as well as the influence of this order on duplex formation (refs. 1–8 and references cited in ref. 8). Most early studies made use of optical techniques such as ultraviolet (UV) and infrared spectroscopy, circular dichroism (CD), and optical rotary dispersion. Other experimental approaches such as NMR, intrinsic viscosity, and sedimentation coefficients also were used, albeit to a lesser extent. In most, but not all, of these studies, the authors interpret their data to be consistent with the existence of some ordered single-stranded structure. Temperature-dependent studies of various equilibrium properties showed the single-stranded structures to "melt" over rather broad temperature ranges compared with higher-order nucleic acid structures (e.g., duplexes, triplexes, etc.). Thermodynamic data were derived indirectly from the temperature-dependent properties by assuming a model for these melting processes (4, 9–13). However, because of the approximations associated with such van't Hoff analyses, as well as difficulties in defining the extent of order in the initial and final states of such broad transitions, the literature contains a rather large range of values for the thermodynamic changes associated with the melting of single-stranded nucleic acid structures (13, 14). This observation is of some concern since, in addition to their intrinsic value as measures of a fundamental biopolymer property, such thermodynamic data are required for a number of important applications [e.g., assessing the validity of various helix-to-coil models by fitting calculated with observed melting curves (9), resolving and interpreting multiphasic transition curves, assigning thermodynamic "baselines" for final "melted" duplex states (12), defining the initial and/or final states in drug binding studies, and predicting the stability and the melting behavior of sequence-specific secondary structures (15)]. Independent of the specific application of interest, the need for sequence- and solution-dependent thermodynamic data on single-stranded

The publication costs of this article were defrayed in part by page charge payment. This article must therefore be hereby marked "*advertisement*" in accordance with 18 U.S.C. §1734 solely to indicate this fact.

Abbreviations: DSC, differential scanning calorimetry; T_m, melting temperature.

*To whom reprint requests should be addressed.

nucleic acid structure(s) has been recognized for some time. Unfortunately, save for a few notable exceptions primarily involving homosequences [particularly oligo(A) and poly(A) sequences], the requisite thermodynamic data have yet to be compiled. As noted above, this deficiency, in part, reflects the difficulties inherent in quantitatively analyzing equilibrium data associated with structures that exhibit very broad thermal transitions.

Recently, however, interest in single-stranded oligonucleotides has been reborn. This rebirth, in part, reflects an explosion of interest in the formation of higher-order DNA structures (e.g., duplexes, triplexes, tetraplexes, etc.) from intra- and intermolecular associations of single strands (16–21), as well as the use of single-stranded oligonucleotides as probes in hybridization strategies designed to form selectively DNA duplex and triplex structures (22, 23). This renewed interest has been fueled by the recognition that hybridizing single strands can be used as selective delivery systems for DNA-cleaving agents, as enhancers of restriction enzyme specificity, as modulators of gene expression, and as indicator probes for the presence of specific single- and double-stranded DNA domains (24–29). Clearly, these uses of single-stranded oligonucleotides have substantial diagnostic and/or therapeutic potentials. However, the design and effective use of selective single-stranded DNA probes and/or delivery systems demands knowledge of the relative affinities that the single strands exhibit under the hybridization conditions for the target DNA domain(s), be they single- or double-stranded (30). Such assessments require sequence and solution-dependent thermodynamic data on the contribution(s) that the initial unhybridized single-stranded oligonucleotides make to duplex, triplex, and even tetraplex formation (12, 15, 21, 30). The experiments described in this report provide the requisite data for one system and demonstrate that the initial state of a single-stranded sequence can make a profound contribution to the formation of a final hybridized complex.

MATERIALS AND METHODS

Oligodeoxyribonucleotide Synthesis and Purification. Oligodeoxyribonucleotides were synthesized using standard solid-phase cyanoethyl phosphoamidite methods (31). Purification of the oligomers was accomplished by HPLC using established protocols (32). HPLC analysis of the nuclease degradation products of the oligomers revealed that each sequence exhibited the expected ratios of nucleotides.

Solution Preparation. All solutions were prepared using a buffer consisting of 10 mM sodium phosphate, 1 mM EDTA, and 1.0 M NaCl, adjusted to pH 7. Oligonucleotide concentrations were determined spectrophotometrically by measuring the absorbance at 260 nm and using the following single-stranded extinction coefficients (ε) at 25°C: $\varepsilon = 1.12 \times 10^5$ $M^{-1}\cdot cm^{-1}$ for S_1 [d(CGCATGAGTACGC)] and $\varepsilon = 1.16 \times 10^5$ $M^{-1}\cdot cm^{-1}$ for S_2 [d(GCGTACTCATGCG)]. Each ε value was determined directly by phosphate analysis (33).

UV Absorption Spectrophotometry. Absorbance versus temperature "melting" profiles of the 13-mer duplex ($S_1\cdot S_2$) and the two component single strands (S_1 and S_2) were measured using a Perkin–Elmer model 575 programmable spectrophotometer equipped with a thermoelectrically controlled cell holder and interfaced to a Tektronix model 4051 computer. Samples were heated and reheated at a rate of 0.1°C/min while the temperature and the absorbance at 260 nm were recorded every 30 sec. For each sample, multiple scans produced superimposable melting profiles. Melting temperatures (T_m) were obtained from these curves using well-established procedures (34). Specifically, for each transition, the shape of the absorbance versus temperature profile was analyzed using extrapolated baselines and a two-state model to calculate a van't Hoff transition enthalpy (ΔH_{vH}) using the relationship $\Delta H_{vH} = (2n + 2)RT_m^2(\delta\alpha/\delta T)_{T_m}$, where α is the fraction of strands in the initial state and n is the transition molecularity. For S_1 only, the entropy change was calculated using the relationship $\Delta S° = \Delta H_{vH}/T_m$. The details of these calculations have been described (35, 36).

CD Spectroscopy. CD spectra were measured using an Aviv model 60DS spectropolarimeter (Aviv Associates, Lakewood, NJ). This instrument is fully computerized, exhibits enhanced sensitivity relative to the original Cary 60 model, and is equipped with a programmable thermoelectrically controlled cell holder.

Differential Scanning Calorimetry (DSC). Calorimetric excess heat capacity (ΔC_p) versus temperature (T) profiles were measured for the duplex and the two component single strands using a Microcal-2 differential scanning calorimeter (Microcal, Northhampton, MA). Calorimetric transition enthalpies ($\Delta H°$) were obtained by integrating the area under the corresponding heat capacity versus temperature profile, since $\Delta H° = \int \Delta C_p dT$. Transition entropies ($\Delta S°$) were determined by measuring the area under the derived $\Delta C_p/T$ versus T, since $\Delta S° = \int (\Delta C_p/T) dT$. The corresponding values of $\Delta G°$ were calculated at 25°C using the standard thermodynamic relationship $\Delta G° = \Delta H° - T\Delta S°$. Significantly, these calorimetrically derived thermodynamic data are model-independent. This feature contrasts with the model-dependent van't Hoff transition enthalpies, which were extracted from the optical data by assuming a two-state melting process. We also derived van't Hoff transition enthalpies from each calorimetric heat capacity curve by analyzing the transition width at the half height (36).

Isothermal Batch Mixing Calorimetry. The batch calorimeter used in this study has been described in detail (37–40). We determined the duplex formation enthalpy at 25°C by mixing in the calorimeter solutions of the two single strands at equal concentrations. The enthalpy for duplex formation is obtained by integrating the area under the resulting heat burst curve and dividing this heat by the number of moles of duplex formed.

RESULTS

UV Spectroscopy. Fig. 1, curve a, shows the 260-nm UV melting curve we have measured for the thermally induced disruption of the 13-mer duplex studied herein. Analysis of the shape of this curve yields a van't Hoff transition enthalpy of 92.2 kcal/mol of duplex (1 cal = 4.184 J), a value consistent

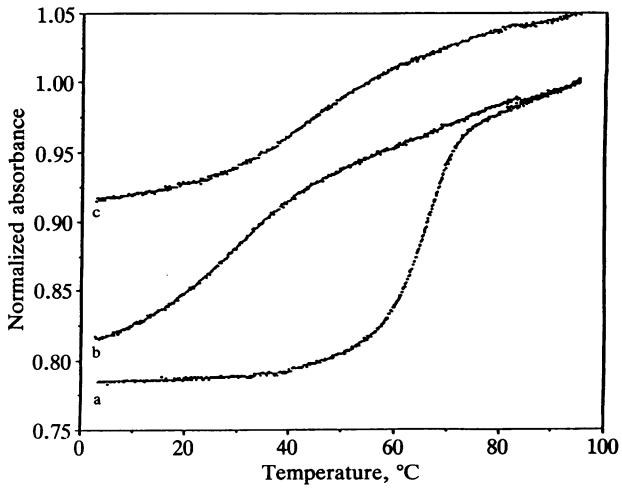

FIG. 1. UV melting curves measured at 260 nm. The 13-mer duplex $S_1\cdot S_2$ at a strand concentration of 7.69 μM (curve a). The S_1 single strand at a strand concentration of 9.01 μM (curve b). The S_2 single strand at a strand concentration of 9.06 μM (curve c). Curve c is displaced by +0.05 absorbance units for ease of display.

with that obtained from the concentration dependence of the duplex T_m (data not shown). Fig. 1, curves b and c, shows the corresponding UV melting curves for the component single strands. Analysis of the shapes of these curves yields van't Hoff transition enthalpies of 29.1 and 26.2 kcal/mol of single strand for S_1 and S_2, respectively. These UV-derived van't Hoff transition enthalpies (ΔH_{vH}^{UV}) are listed in Table 1 along with the corresponding melting temperatures, T_m. In contrast to the 13-mer duplex, the T_m values for the single-strand transitions do not depend on strand concentration over a concentration range of 9.06×10^{-6} to 5.72×10^{-4} M in single strand. The fact that the T_m values for S_1 and S_2 are invariant upon a concentration change in excess of 100-fold is consistent with these transitions being monomolecular.

CD Spectroscopy. We have measured CD spectra as a function of temperature for the S_1 and S_2 single strands. At 25°C, the temperature of the initial and final states in the isothermal batch mixing calorimetric measurement, both single strands exhibit CD spectra characteristic of ordered structure. At ≈80°C, the temperature of the final state(s) in the DSC measurement, the CD spectra for S_1 and S_2 exhibit altered shapes and reduced intensities characteristic of final states in which the ordered structure present at 25°C has been thermally disrupted (1, 3, 41). These observations are consistent with the corresponding UV melting curves of the single strands (see Fig. 1). Furthermore, the CD profiles of S_1 and S_2 do not change with strand concentration, thereby suggesting that the ordered structure within each single strand is formed monomolecularly. Based on these observations, we interpret the shapes and temperature dependences of the CD profiles as reflecting intramolecular single-strand base-stacking interactions. This interpretation is consistent with previous CD studies of single-stranded structures (refs. 1, 3, and 41 and references cited in ref. 41).

DSC Curves. Fig. 2 shows the calorimetric heat capacity curves for the 13-mer duplex (curve a) and for S_2, one of its component single strands (curve b). Sufficient amounts of S_1 were not available to conduct a DSC measurement on its thermally induced melting.

For each transition, a calorimetric transition enthalpy (ΔH_{cal}^{DSC}) was obtained directly from the area under the experimental ΔC_p versus T curve. These data are listed in Table 2. The corresponding calorimetrically derived van't Hoff transition enthalpies (ΔH_{vH}^{cal}) also were determined from the experimental heat capacity curves by analyzing the transition widths (36). These van't Hoff transition enthalpies are listed in Table 1. Note that for each transition, the excess heat capacity of the final state is about equal to that of the initial state (e.g., the pre- and post-transition baselines have nearly the same heat capacity values). This observation indicates that the melting of the duplex and the S_2 single strand is accompanied by little, if any, net change in heat capacity.

Table 1. van't Hoff transition enthalpies (ΔH_{vH}) and melting temperatures (T_m) associated with the melting of the 13-mer duplex $S_1 \cdot S_2$ and its component single strands

DNA	T_m, °C	ΔH_{vH}^{UV}, kcal/mol	ΔH_{vH}^{cal}, kcal/mol
$S_1 \cdot S_2$	74.0*	92.2	104.1
S_1	29.6	29.1	—
S_2	45.5	26.2	24.9

ΔH_{vH}^{UV} was derived from the shapes of the UV melting curves (see ref. 36 for details). ΔH_{vH}^{cal} was derived from the shapes of the calorimetric heat capacity curves (see ref. 36 for details).
*Corresponds to a strand concentration of 0.435 mM. At the 7.69 μM strand concentration used in the duplex optical melting study, T_m equals 63.8°C.

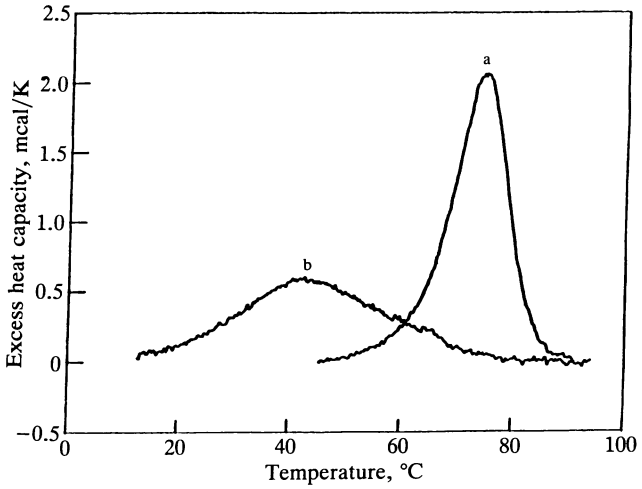

FIG. 2. Calorimetric excess heat capacity (ΔC_p) versus temperature (T) curves for the 13-mer duplex $S_1 \cdot S_2$ at a strand concentration of 0.435 mM (curve a) and for the S_2 single strand at a strand concentration of 0.572 mM (curve b).

Isothermal Batch Mixing Calorimetry. We have measured the calorimetric heat burst curve that results upon the equimolar mixing of S_1 and S_2 at 25°C to form the 13-mer duplex. From the area under the heat-burst curve and the known strand concentrations, we calculated ΔH_{cal}^{batch}, the calorimetric enthalpy for duplex formation at 25°C. This value is listed in Table 2.

Complete Thermodynamic Profiles. $\Delta G°$ and $\Delta S°$ can be calculated from the calorimetric and optical measurements. The resulting complete thermodynamic profiles are listed in Table 3.

DISCUSSION

Inspection of the calorimetrically measured enthalpy data listed in Table 2 reveals a large disparity between ΔH_{cal}^{batch}, the enthalpy for duplex formation (−56.4 kcal/mol) at 25°C, and ΔH_{cal}^{DSC}, the enthalpy for duplex disruption (117 kcal/mol) at 74°C, the duplex melting temperature. Since as noted above, the net heat capacity change for duplex disruption is close to zero (see Fig. 2), we cannot rationalize the enthalpy difference between duplex formation at 25°C and duplex disruption at 74°C in terms of a heat capacity effect. Instead, we focus our attention on potential differences in the single-stranded states at 25°C and ≈80°C, the initial and final temperatures of the batch and DSC experiments, respectively.

To assist us in assessing the origin of the disparity we observe in the magnitudes of the enthalpies for duplex formation and disruption, we have constructed the thermodynamic cycle shown below:

$$\begin{array}{ccc} \text{Duplex (5°C)} & \xrightarrow[\Delta H_1]{} & S_1\ (80°C) + S_2\ (80°C) \\ \downarrow \Delta H_2 & & \uparrow \Delta H_4 \\ \text{Duplex (25°C)} & \xrightarrow{\Delta H_3} & S_1\ (25°C) + S_2\ (25°C) \end{array}$$

Table 2. Calorimetrically measured enthalpies for the melting (ΔH_{cal}^{DSC}) and the formation (ΔH_{cal}^{batch}) of the 13-mer duplex $S_1 \cdot S_2$ and its component single strands, S_1 and S_2

Process	T_m,°C	ΔH_{cal}^{DSC}, kcal/mol	ΔH_{cal}^{batch}, kcal/mol
Duplex formation	25.0	—	−56.4
Duplex melting	74.0	117.0	—
S_2 melting	45.5	27.2	—

Table 3. Complete thermodynamic profiles for the melting of the 13-mer duplex $S_1 \cdot S_2$ and its component single strands, S_1 and S_2

Process	T_m, °C	$\Delta G°$ (25°C), kcal/mol	$\Delta H°$, kcal/mol	$\Delta S°$, cal·degree^{-1}·mol^{-1}	$T\Delta S°$, kcal/mol
Duplex melting	74.0*	20.0	117.0	325.4	97.0
S_1 melting	29.6	0.45	29.1	96.1	28.6
S_2 melting	45.5	1.44	27.2	86.4	25.8

Data for S_1 melting was derived from the UV melting curve. All other data were derived from calorimetric measurements. The $\Delta H°$ and $\Delta S°$ data listed do not predict the measured T_m values due to the random experimental error inherent in all such independent determinations of these parameters. *Corresponds to a strand concentration of 0.435 mM.

ΔH_1 corresponds to ΔH_{cal}^{DSC}, the transition enthalpy we measure directly using DSC, and is equal to +117 kcal/mol of duplex. ΔH_3 corresponds to $-\Delta H_{cal}^{batch}$, the negative of the duplex formation enthalpy we measure directly using batch calorimetry, and is equal to +56.4 kcal/mol of duplex. ΔH_2 is equal to zero since our DSC profile reveals no enthalpy change in heating the duplex from 5 to 25°C. ΔH_4 is the sum of the integral enthalpy changes associated with the heating of each single strand from 25 to 80°C. For S_2, we have measured this value directly using DSC (Fig. 2) and indirectly using UV melting (Fig. 1). These values, ΔH_{cal}^{DSC} (S_2) and ΔH_{vH}^{UV} (S_2), are listed in Tables 1 and 2. Note that both methods yield very similar transition enthalpies. Inspection of the heat capacity curve for S_2 (Fig. 2) reveals that the transition is just beginning to occur at 25°C. Consequently, for the integral melting of S_2 from 25 to 80°C, we assign the total enthalpy change of 27.2 kcal/mol [ΔH_{cal}^{DSC} (S_2)] that we measure directly by DSC. For S_1, we determined a total transition enthalpy of −29.1 kcal/mol from the UV melting curve shown in Fig. 1 [see ΔH_{vH}^{UV} (S_1) in Table 1]. As noted above, we did not possess sufficient quantities of S_1 to conduct the corresponding DSC measurement. However, the excellent agreement between the DSC and UV transition enthalpies for S_2 gives us confidence in assigning the van't Hoff value of 29.1 kcal/mol to the overall melting of S_1. The corresponding integral transition enthalpy relevant to the thermodynamic cycle can be approximated from the UV melting curve by correcting the total transition enthalpy for that fraction which already has occurred by 25°C. This treatment yields an integral transition enthalpy of 23.6 kcal/mol for the melting of S_1 from 25 to 80°C. Thus, the overall value of ΔH_4 is 50.8 kcal/mol, the sum of the integral transition enthalpies for S_1 (23.6 kcal/mol) and S_2 (27.2 kcal/mol).

Based on the thermodynamic cycle shown above, $\Delta H_1 = \Delta H_2 + \Delta H_3 + \Delta H_4$. Thus, we can calculate a predicted value for ΔH_1 ($\equiv \Delta H_{cal}^{DSC}$) by adding the values for ΔH_2, ΔH_3 ($\equiv -\Delta H_{cal}^{batch}$), and ΔH_4. Using the experimental values (in kcal/mol), we obtain: $\Delta H_1 = 0 + [-(-56.4)] + [(23.6 + 27.2)] = 107.2$ kcal/mol. This predicted value of 107.2 kcal/mol for ΔH_1 should be compared with the corresponding experimental value of 117.0 kcal/mol that we measure directly using DSC. This agreement is good and lends support to our analysis and interpretation of the data as described above.

In summary, the substantial difference in the magnitudes of the enthalpy changes that we measure for duplex formation by batch calorimetry (−56.4 kcal/mol) and duplex disruption by DSC (+117 kcal/mol) can be rationalized in terms of differences in the enthalpy states of the single strands at 25°C and 80°C. This dramatic effect suggests that near room temperature, single strands can possess order that enthalpically (albeit not necessarily structurally) prepare them for duplex formation. In fact, prior to association at 25°C, the two complementary single strands studied here already possess >40% (50.8/117) of the total enthalpy that ultimately stabilizes the final duplex state. This feature of single-stranded structure near room temperature could significantly reduce the total enthalpic driving force that one might predict for duplex formation from simple nearest-neighbor data (which generally are derived from measurements in which the single strands are in their random-coil states). Consequently, potential contributions from single-stranded structure must be recognized and accounted for when designing hybridization experiments and when using titration and/or batch mixing techniques to study the formation of duplexes and higher-order structures (e.g., triplexes, tetraplexes, etc.) from their component single strands.

Complete Thermodynamic Profiles. Complete thermodynamic profiles for the melting of both the duplex and the single-stranded states are listed in Table 3. Inspection of the data for the single strands reveals that, despite rather substantial transition enthalpies [ΔH_{vH}^{UV} (S_1) = 29.1 kcal/mol, ΔH_{cal}^{DSC} (S_2) = 27.2 kcal/mol], the single-stranded structures are only marginally stable at 25°C [ΔG (S_1) = 0.45 kcal/mol; ΔG (S_2) = 1.44 kcal/mol]. This feature results from large enthalpy–entropy compensations that yield small free energies of stabilization. By contrast, the duplex state is dramatically stable at 25°C ($\Delta G° = 20.0$ kcal/mol), since the greater transition enthalpy of the duplex ($\Delta H° = 117.0$ kcal/mol) more than compensates for the favorable entropy of duplex disruption ($\Delta S° = 325.4$ cal·degree^{-1}·mol^{-1}). Thus, even though the two single strands exhibit a total transition enthalpy in excess of 40% of the duplex transition enthalpy (50.8/117), the extrapolated free energies for the two single strands at 25°C amount to only about 10% (1.89/20.0) of the total free energy of the duplex at 25°C.

Nature of the Transitions. Inspection of the data in Tables 1 and 2 reveals that for the melting of both the 13-mer duplex and S_2 the directly measured calorimetric transition enthalpy (ΔH_{cal}^{DSC}) and the corresponding calorimetrically derived van't Hoff transition enthalpy (ΔH_{vH}^{cal}) are similar, exhibiting ratios of about 1.1. The fact that these ratios have values close to unity indicates that the melting of both the 13-mer duplex and the S_2 single strand occur in a nearly two-state manner (36, 42, 43). This observation justifies our use of a two-state model for the van't Hoff analyses of our optical and calorimetric data melting data. In the absence of DSC data for S_1, we have assumed that it exhibits similar two-state melting behavior.

Single-Stranded Nearest-Neighbor Interactions. By analogy with analyses of duplex structures, it is of interest to consider the single-stranded structures studied herein in terms of nearest-neighbor interactions. For the 13-mer single-strands S_1 and S_2, this analysis simply requires one to divide each of the thermodynamic parameters listed in Table 3 by 12, the number of pair-wise neighbor interactions. This exercise, which assumes a linear array of bases for the initial ordered state, yields the following average single-stranded nearest-neighbor interactions: $\Delta g° = 0.04$ kcal/mol; $\Delta h° = 2.4$ kcal/mol; $\Delta s° = 8.0$ cal·degree^{-1}·mol^{-1} for S_1; and $\Delta g° = 0.12$ kcal/mol; $\Delta h° = 2.27$ kcal/mol; $\Delta s° = 7.20$ cal·degree^{-1}·mol^{-1} for S_2. (The lower-case letters are used to indicate that the thermodynamic values correspond to average pair-wise interactions.) Significantly, these enthalpy val-

ues compare favorably with those previously measured calorimetrically over a similar temperature interval for single-stranded nucleic acid structures composed entirely of either adenine or cytosine residues (6, 14, 44–47), although the exact interpretation of the nature of the overall single-strand transition varies from study to study. In connection with the analysis employed here, we recognize the formal possibility that the initial single-stranded states may form hairpins. However, based on the primary sequences, the CD spectra (and their temperature dependences), and NMR data on the single strands (R. Jin and K.J.B., unpublished results), we consider hairpin formation by the initial single-stranded state to be unlikely. More significantly, our thermodynamic analysis of the single-stranded melting events requires only that the structures formed by the initial states be monomolecular, a requirement consistent with the concentration-independent nature of the transitions. Even for systems in which hairpins exist in solution, their formation would not alter the conclusion that single-stranded DNA structure (whether a linear array of bases, a hairpin, or any other intramolecular structure) can contribute significantly to the thermodynamics of duplex formation.

Concluding Remarks. We have demonstrated that at 25°C single-stranded DNA sequences can possess considerable order that can significantly influence the thermodynamic driving forces associated with duplex formation. This feature must be recognized and accounted for when designing single-strand probes for selective hybridization experiments and when interpreting data associated with the formation of higher-order DNA structures (e.g., duplexes, triplexes, tetraplexes, etc.) from inter- and/or intramolecular associations of single strands.

K.J.B. dedicates this paper to Sherrie Schwab for demonstrating to him the significant contribution that a single strand can make to the stability of a duplex. This work was supported by National Institutes of Health Grants GM23509 and GM34469 and by a grant from the Busch Memorial Research Fund.

1. Holcomb, D. N. & Tinoco, I., Jr. (1965) *Biopolymers* **3,** 121–133.
2. Leng, M. & Felsenfeld, G. (1966) *J. Mol. Biol.* **15,** 455–466.
3. Brahms, J., Michelson, A. M. & van Holde, K. E. (1966) *J. Mol. Biol.* **15,** 467–488.
4. Poland, D., Vournakis, J. N. & Scheraga, H. A. (1966) *Biopolymers* **4,** 223–235.
5. Felsenfeld, G. & Miles, H. T. (1967) *Annu. Rev. Biochem.* **36,** 407–448.
6. Rawitscher, M. A., Ross, P. D. & Sturtevant, J. M. (1963) *J. Am. Chem. Soc.* **85,** 1915–1918.
7. Stanard, B. S. & Felsenfeld, G. (1975) *Biopolymers* **14,** 299.
8. Saenger, W. (1984) in *Principles of Nucleic Acid Structure*, Springer Advanced Texts in Chemistry, ed. Cantor, C. R. (Springer, New York), pp. 302–315.
9. Applequist, J. & Damle, V. (1966) *J. Am. Chem. Soc.* **88,** 3895–3900.
10. Pörschke, D. (1971) *Biopolymers* **10,** 1989–2013.
11. Powell, J. T., Richards, E. G. & Gratzer, W. B. (1972) *Biopolymers* **11,** 235–250.
12. Appleby, D. W. & Kallenbach, N. R. (1973) *Biopolymers* **12,** 2093–2120.
13. Davis, R. C. & Tinoco, I., Jr. (1968) *Biopolymers* **6,** 223–242.
14. Breslauer, K. J. & Sturtevant, J. M. (1977) *Biophys. Chem.* **7,** 205–209.
15. Breslauer, K. J., Frank, R., Blöcker, H. & Marky, L. A. (1986) *Proc. Natl. Acad. Sci. USA* **83,** 3746–3750.
16. Puglisi, J. D., Wyatt, J. R. & Tinoco, I., Jr. (1988) *Nature (London)* **331,** 283–286.
17. Erie, D. A., Sinha, N. K., Olson, W. K., Jones, R. A. & Breslauer, K. J. (1987) *Biochemistry* **26,** 7150–7159.
18. Erie, D. A., Sinha, N. K., Olson, W. K., Jones, R. A. & Breslauer, K. J. (1989) *Biochemistry* **28,** 268–273.
19. Sklenár, V. & Feigon, J. (1990) *Nature (London)* **345,** 836–838.
20. Häner, R. & Dervan, P. B. (1990) *Biochemistry* **29,** 9761–9765.
21. Jin, R., Breslauer, K. J., Jones, R. A. & Gaffney, B. L. (1990) *Science* **250,** 543–546.
22. Moser, H. E. & Dervan, P. B. (1987) *Science* **238,** 645–650.
23. Hanvey, J. C., Shimizu, M. & Wells, R. D. (1990) *Nucleic Acids Res.* **18,** 157–161.
24. Povsic, T. J. & Dervan, P. B. (1989) *J. Am. Chem. Soc.* **111,** 3059–3061.
25. Strobel, S. A., Moser, H. E. & Dervan, P. B. (1988) *J. Am. Chem. Soc.* **110,** 7927–7929.
26. François, J.-C., Saison-Behmoaras, T., Barbier, C., Chassignol, M., Thoung, N. T. & Hélene, C. (1989) *Proc. Natl. Acad. Sci. USA* **86,** 9702–9706.
27. Prasenth, D., Perroualt, L., Doan, T. L., Chassignol, M., Thoung, N. & Hélène, C. (1988) *Proc. Natl. Acad. Sci. USA* **85,** 1349–1353.
28. Sun, J.-S., François, J.-C., Montenay-Garestier, T., Saison-Behmoaras, T., Roig, V., Thoung, N. T. & Hélène, C. (1989) *Proc. Natl. Acad. Sci. USA* **86,** 9198–9202.
29. Maher, L. J., III, Wold, B. & Dervan, P. B. (1989) *Science* **245,** 725–730.
30. Plum, G. E., Park, Y. W., Singleton, S. F., Dervan, P. B. & Breslauer, K. J. (1990) *Proc. Natl. Acad. Sci. USA* **87,** 9436–9440.
31. Sinha, N. D., Biernat, J. & Köster, M. (1983) *Tetrahedron Lett.* **24,** 5843–5846.
32. Gaffney, B. L. & Jones, R. A. (1989) *Biochemistry* **28,** 5881–5889.
33. Snell, F. D. & Snell, C. T. (1949) *Colorimetric Methods of Analysis* (Van Nostrand, New York), Vol. 2.
34. Breslauer, K. J. (1986) in *Thermodynamic Data for Biochemistry and Biotechnology*, ed. Hinz, H. (Academic, New York), pp. 377–399.
35. Breslauer, K. J., Sturtevant, J. M. & Tinoco, I., Jr. (1975) *J. Mol. Biol.* **99,** 549–565.
36. Marky, L. A. & Breslauer, K. J. (1987) *Biopolymers* **26,** 1601–1620.
37. Marky, L. A., Curry, J. & Breslauer, K. J. (1985) in *Molecular Basis of Cancer*, ed. Rein, R. (Liss, New York), pp. 155–173.
38. Marky, L. A., Snyder, J. G., Remeta, D. P. & Breslauer, K. J. (1983) *J. Biomol. Struct. Dyn.* **1,** 487–507.
39. Pennington, S. N. & Brown, H. D. (1969) in *Biochemical Microcalorimetry*, ed. Brown, H. D. (Academic, New York), pp. 207–219.
40. Mudd, C., Berger, R. L., Hopkins, H. P., Friauf, W. S. & Gibson, C. J. (1982) *Biochem. Biophys. Methods* **6,** 179–203.
41. Bush, C. A. (1974) in *Basic Principles in Nucleic Acid Chemistry*, ed. Ts'o, P. O. P. (Academic, New York), Vol. 2, pp. 91–169.
42. Sturtevant, J. M. (1987) *Annu. Rev. Phys. Chem.* **38,** 463–488.
43. Privalov, P. L. & Potekhin, S. A. (1986) *Methods Enzymol.* **131,** 4–51.
44. Suurkuusk, J., Alvarez, J., Freire, E. & Biltonen, R. (1977) *Biopolymers* **16,** 2641–2652.
45. Filimonov, V. V. & Privalov, P. L. (1978) *J. Mol. Biol.* **122,** 465–470.
46. Freier, S. M., Hill, K. O., Dewey, T. G., Marky, L. A., Breslauer, K. J. & Turner, D. H. (1981) *Biochemistry* **20,** 1419–1426.
47. Neumann, E. & Ackermann, Th. (1969) *J. Phys. Chem.* **73,** 2170–2178.